Article

Tri-Generation System Configuration Selection Based on Energy and Exergy Analyses

Tuananh Bui [1,2], Young-Sang Kim [1,2,*], Dong-Keun Lee [1], Kook-Young Ahn [1,2] and Sang-Min Lee [1]

[1] Department of Zero-Carbo Fuel & Power Generation, Korea Institute of Machinery & Materials (KIMM), 156 Gajeongbuk-ro, Yuseong-gu, Daejeon 34103, Korea

[2] Environment·Energy Machinery217, KIMM Campus, University of Science and Technology (UST), Gajeongro, Yuseong-gu, Daejeon 34113, Korea

* Correspondence: yskim@kimm.re.kr

Abstract: A tri-generation system combining cooling, heating, and power generation can contribute to increased system efficiency and thereby reduce greenhouse gas emissions. This study proposed a novel concept using 100-kW polymer electrolyte membrane fuel cells (PEMFCs) as the basis for a tri-generation system with an integrated heat pump and adsorption chiller for greenhouse use. Three configurations of heat pump loop were designed to recover the waste heat from PEMFCs and used either for direct heating or cooling power generation in adsorption cooling. Analyses were carried out in terms of primary energy rate (PER) and exergy efficiencies. Of those investigated, the layout with a heat pump and internal heat exchanger demonstrated the best performance, with PERs of the cooling and heating modes at 0.94 and 0.78, respectively. Additionally, the exergy analysis revealed that the exergies are mostly destroyed at the expansion valve and evaporator due to differences in pressure and temperature. These differences are minimized when the system layout contains a cascade heat pump loop or an internal heat exchanger, thus resolving the problem of exergy destruction. As a result, the total exergy destruction in the system was decreased from 61.11% to 49.18% and 46.60%, respectively. Furthermore, the proposed configurations showed 36.1% and 31.4% lower values in terms of energy consumption compared with relevant works in the heating mode and cooling mode, respectively.

Keywords: tri-generation; polymer electrolyte membrane fuel cell; PEMFCs; exergy; greenhouse

1. Introduction

In recent years, climate change has been become increasingly severe due to increasing greenhouse gas emissions. Under this pressure, along with the need to find new, cleaner, and more sustainable energy sources, the efficiency of energy systems must be improved by recovering waste heat, such as through fuel-cell-based tri-generation plants.

In fuel-cell-based tri-generation plants, the waste heat from a fuel cell is used to supply heat and run the heat-driven refrigeration cycle to produce cooling power. There are many studies [1–7] of tri-generation systems focusing on fuel cells with high-quality waste heat sources, such as phosphoric acid fuel cells, molten carbonate fuel cells, and solid-oxide fuel cells, whereas their coupling with low-temperature fuel cells is relatively untapped [8]. Additionally, according to [9], more than 80% of the total estimated waste heat in the United States is in the 77–300 °F (25–149 °C) temperature range. Though low-temperature waste heat is low quality, it is present in sufficiently large magnitudes that its work potential exceeds that of higher-temperature sources [9].

Baniasadi et al. investigated 10 kW polymer electrolyte membrane fuel cells (PEMFCs) based on exegetic and exergoeconomic evaluations [10]. It was concluded that besides operating pressure and temperature, fuel cell voltage can significantly affect the exergy cost of the system. In addition, with an increase in the heat source temperature, the exergy

cost of chilled water decreases and the coefficient of performance (COP) of the absorption chiller increases by more than 30%.

Chen et al. also studied a 5 kW PEMFCs-based residential tri-generation system with absorption chiller [11]. The maximum efficiencies of the system were 70.1% in summer, and 82% in winter.

In tri-generation systems or multi-generation systems, heat pumps were also used to upgrade heat quality by increasing their temperature before instant use or storage. Khan et al. developed a novel solar-assisted multi-generation system using high-temperature phase-change material [12]. The heat pump was used to absorb heat from exhaust gas, then reject desired heat to maintain the suitable temperature for the required heated area.

Bellos et al. used a multi-layer heat pump to pump heat captured from ambient air to several desired temperatures and store them for further uses [13]. Electricity supplied for the heat pump was volatile electricity from renewable energy sources. The stored heat could be reconverted to electricity by using the Rankine cycle or direct uses such as space heating and hot-water production. In addition, the system also produced cold storage at 0 °C for cooling.

Kim et al. studied a hybrid solar geothermal heat pump poly-generation system using a water-to-water heat pump [14]. The design was demonstrated in Cheongju, Korea. The heating load was 13.8 kW at an ambient temperature of −10.3 °C whereas the cooling load was 10.6 kW at an ambient temperature of 32.3 °C. Its performance was compared with a software-simulated design result.

As can be seen, the PEMFCs-based tri-generation system has been studied in the literature; however, low-temperature PEMFCs have not received much attention compared with high-temperature fuel cells in tri-generation systems because of low-temperature waste heat, whereas a heat pump was used widely in tri-generation or multi-generation systems to upgrade heat quality for either direct heating or other purposes.

As a novelty, this study proposes the combination of PEMFCs and a heat pump in a tri-generation system in which PEMFCs produce electricity, and the heat pump absorbs waste heat from the PEMFCs in order to increase its temperature for hot-water storage. This hot water can be for direct use or for cooling power production using an adsorption chiller. The tri-generation system is designed for a 4800 m^2 greenhouse where electricity is required for lighting; heating is for winter and cooling is for summer.

2. System Description and Parameters Used for Simulation

2.1. System Description

The main components of the proposed tri-generation system are PEMFCs, a heat pump loop, an adsorption chiller, and an electric heat pump (EHP), described in Figure 1. Natural gas is reformed in a steam reformer to obtain pure hydrogen for the PEMFCs stack. In typical PEMFCs-based tri-generation systems [8,15], the temperature of the output water is in the range of 50–60 °C, which is suitable only for direct residential use but considered relatively low for use in heat-driven adsorption chillers, where the temperature is normally 60–95 °C. Consequently, in this study, the heat pump loop is used to utilize the waste heat of 55 °C cooling water exhausted from PEMFCs whereas the EHP is employed to produce the remaining amount of required heat and cooling power for the greenhouse. Cooling water is heated to the rated inlet temperature of 70 °C of a commercial adsorption chiller [16]. An electric heater can be used to elevate the temperature, but converting electricity to low-temperature heat is not generally given consideration due to its inefficiency. This study proposes the use of three heat pump loops in the design to bridge the temperature gap between the PEMFCs and the adsorption chiller, as shown in Figure 1. Based on energy and exergy analyses [17], the performances of the candidate layouts are evaluated for comparison and selection. Inclusion of a heat pump in the system is suggested because it can bring heat from a low-temperature source into a higher-temperature space [18], with the direction being opposite to that of natural heat transfer. Moreover, a heat pump can deliver an amount of heat equivalent to 3–5 times the consumed power.
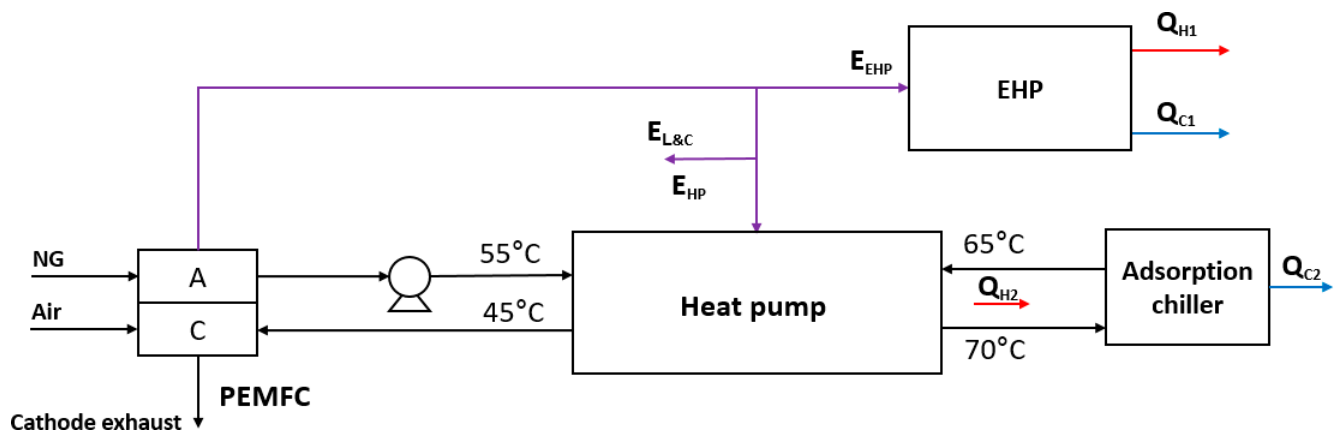
Figure 1. The layout of the proposed tri-generation system.

As discussed, a heat pump is more efficient than a heater; however, the performance of a heat pump is predominantly dependent on the refrigerant and operating pressure. As the adsorption chiller requires an input temperature of 70 °C, the refrigerant must operate at temperatures higher than 70 °C, with subsequent condensation at 70 °C at an appropriate pressure. Of the common refrigerants, R134a, R22, and R152a are the three most suitable candidates. According to Bellos et al., R152a is the cheapest refrigerant; its thermodynamic characteristics are also superior to those of R134a [19]. For instance, the energy efficiency of a refrigeration system is 20% higher if it uses R152a instead of R134a. Furthermore, for condensation at 70 °C, R152a requires the lowest compressed pressure, as shown in Table 1. Essentially, R152a also has the lowest environmental impact of the three refrigerants. Following consideration of all the aforementioned factors, R152a was selected as the refrigerant for the heat pump layouts in this study.

Table 1. Refrigerant characteristics.

Refrigerant Candidates	R134a	R22	R152a
Comp. Outlet Pressure (bar)	41	30	20
Ozone Depletion Potential (ODP)	0	0.05	0
Global Warming Potential (GWP)	1300	1700	120

2.2. System Scale, Assumptions, and Specifications

In the present study, a 100 kW PEMFCs-based tri-generation system was used to supply electricity, heat, and cooling power for a greenhouse, described in Figure 1. The maximum heat load of the greenhouse is calculated using Equation (1).

$$Q_{max} = A_g U(T_{in} - T_{out})(1 - f_r) \tag{1}$$

where Q_{max} is the maximum heat load (kW), A_g is the greenhouse surface area (m^2), U is the heating load factor of glass greenhouses (kW/(m^2 °C)), T_{in} is the indoor temperature (°C), T_{out} is the outdoor temperature (°C), and f_r is the thermal energy saving rate due to thermal insulation coating. The efficiency of the PEMFCs stack was assumed to be 50%, a commonly used value. The PEMFCs mentioned in this study are a complete PEMFCs module including a fuel cell stack, reformer, burner, and filter. It is fueled by natural gas and the calculated efficiency is 37.1%. An adsorption chiller is used to supply cooling power for the greenhouse by utilizing waste heat of cooling water exhausted from the PEMFCs. The rated power output of the adsorption chiller is 72 kW, and the design COP is 0.5 [15]. The remaining required cooling power and heat are supplied by a commercial electric heat pump (EHP) [20]. Other assumptions and specifications used for the system simulation are listed in Table 2.

Table 2. Assumptions and specifications for system simulation.

Component	Specification	Unit	Value
Tri-generation system	Lighting and control load	kW	10
PEMFCs module	Capacity	kW	25
	Operating temperature	°C	65
	Fuel type	-	NG
	Stack electrical efficiency	%	50
	Stack conversion rate	-	1
	Heat to cooling water	%	35
	Heat to cathode off-gas	%	5
	Heat to anode off-gas	%	10
	Heat loss	%	20
	Voltage	V	1.2
	Cooling water input temperature	°C	45
	Cooling water output temperature	°C	55
	Water pump isentropic efficiency	%	70
Adsorption chiller	Coefficient of performance (COP)	-	0.5
	Rated output power	kW	72
	Rated water inlet temperature	°C	70
	Rated water outlet temperature	°C	65
Greenhouse	Surface area	m^2	4800
	Heating load factor of glass greenhouse	$kW/(m^2 \, °C)$	0.00616
	Winter indoor temperature	°C	15
	Winter outdoor temperature	°C	−15
	Summer indoor temperature	°C	25

2.3. Proposed Layouts and Description

The first proposed layout with a simple heat pump (case A) is described in Figure 2. The 55 °C cooling water, stream 7, exiting from the PEMFCs, transfers heat to the refrigerant in the main evaporator, EV1, and is cooled to 45 °C before returning to the fuel cell. The gaseous refrigerant, stream 16, is pressurized to 20 bar and circulated through the system by compressor C1. The highly pressurized refrigerant, stream 17, is cooled down by 65 °C water, stream 14, in condenser CD1. The condensed refrigerant, stream 18, then passes through the expansion valve, V1, where it loses pressure and partially vaporizes. The low-pressure (3.7 bar) refrigerant stream enters the sub-evaporator, EV2, and main evaporator, EV1, to gain heat from water, stream 7, and then completely vaporizes before arriving at the compressor for a new loop. In the condenser, the 65 °C water receives heat from the refrigerant, is heated to 70 °C, stream 15, and is then ready to enter adsorption chiller to generate cooling power, Q_{C2}. In addition, 25 °C water, stream 9, releases heat to the refrigerant in EV2, is cooled to 15 °C, and provides additional cooling power, Q_{C3}, to the system.

In order to reduce the compression work of the heat pump loop, the second proposed layout (case B), with a cascade layout, is introduced in Figure 3. The sub-evaporator in the first proposal is replaced by a cascade heat pump loop. The low and high pressure values in the cascade heat pump loop are 3.7 and 11 bar, respectively; the low pressure in the main loop is increased to 9 bar, with the compression ratio reduced from 5.4 in case A to 2.2 in case B. Consequently, there is a decrease in compression work.

Figure 2. Proposed layout with a simple heat pump (case A).

Figure 3. Proposed layout with a cascade heat pump loop (case B).

Figure 4 shows the final proposed layout (case C), which aims to increase the overall system efficiency by recuperating heat from a high-temperature stream. Though heat is transferred to water in CD1, the temperature of stream 19 is still relatively high compared with those of other streams in the system. Therefore, it is split into two streams. The main stream, stream 20, enters the expansion valve V1, decreases in pressure and temperature, and then increases in temperature by gaining heat from the sub-stream, stream 24. The remaining stream passes through expansion valve V2, absorbs heat at EV2, vaporizes, becomes compressed, and then mixes with stream 18 before entering the main compressor, C1.
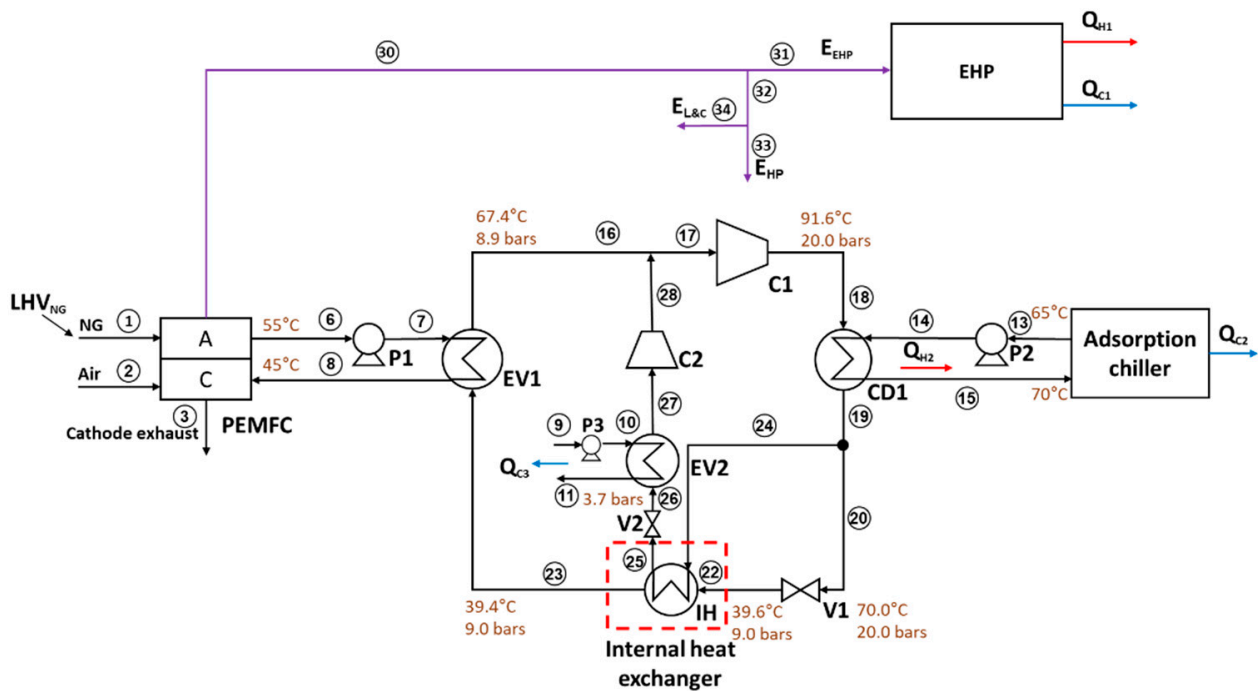
Figure 4. Proposed layout with an internal heat exchanger (case C).

3. Methodology

3.1. Energy Analysis

The conventional method for the energetic evaluation of a heating or cooling system is based on the coefficient of performance (COP). However, this method is not suitable in the case of a tri-generation system, where electricity is one of the outputs. Instead, the primary energy rate (PER) is widely used as the decisive value for energetic analysis [21–25]. The PER is defined as the ratio of primary energy demand to energy outputs, including heating, cooling, and electricity. Consequently, the system with the lowest PER is the best system with regard to energy consumption [25]. In this study, PER was calculated according to Equation (2).

$$\text{PER} = \text{LVH}_{NG}/(E_{L\&C} + Q_H + Q_C) \tag{2}$$

where PER is the primary energy rate, LHV_{NG} is the low-heat value of natural gas input to the system, $E_{L\&C}$ is the electricity for lighting and control, Q_H is the total heating power output, and Q_C is the total cooling power output.

3.2. Exergy Analysis

Exergy is defined as the maximum theoretical useful work that can be obtained as the systems interact while proceeding to equilibrium in which heat transfer only occurs with the environment [20]. The total exergy (E) can be divided into four components of physical exergy (E_{PH}), chemical exergy (E_{CH}), potential exergy (E_{PT}), and kinetic exergy (E_{KN}). In the scope of this study, only the exergy in the heat pump cycle was calculated for comparison among proposals. Consequently, the chemical exergy can be neglected because there is no chemical reaction in the heat pump loops. In addition, the potential and kinetic exergies can also be ignored [20] because the systems are at rest and located at low altitudes. Consequently, only physical exergy is quantified and evaluated.

In the exergy analysis, the exergy of product (E_P) and the exergy of fuel (E_F) are defined for each component. The exergy destruction (E_D) is then calculated according to the exergy balance, as shown in Equation (3). At the system level, the exergy loss (E_L) should be considered in the exergy balance, as described by Equation (4).

$$E_{D,k} = E_{F,k} - E_{P,k} \tag{3}$$

$$E_{D,tot} = E_{F,tot} - E_{P,tot} - E_{L,tot} \tag{4}$$

The exegetic efficiency is defined as the ratio of the exergy of product to the exergy of fuel, as defined by Equations (5) and (6).

1. Component level:

$$\varepsilon_k = E_{P,k}/E_{F,k} = 1 - (E_{D,k}/E_{F,k}) \tag{5}$$

2. System level:

$$\varepsilon_{tot} = E_{P,tot}/E_{F,tot} = (E_{F,tot} - (E_{D,tot} + E_{L,tot}))/E_{F,tot} \tag{6}$$

The exergy destruction ratio shows the distribution of exergy destruction over each component within the system, which is calculated using Equation (7). For the throttle valves, only exergy destruction is considered. In this study, 0 °C and 1 atm were selected as reference states for exergy calculation.

$$y_k = E_{D,k}/E_{F,tot} \tag{7}$$

In the systems in which several configurations are proposed for selection, in addition to energy efficiency, exergy efficiency is another valuable indicator to justify the performance of the system. Javadi et al. used exergy analysis combined with energy, economic, and environmental analyses to compare three configurations of a combined-cycle power plant integrated with a solar power tower system [26]. Hasani et al. used exergy destruction rate, net present value, and exergy flow diagrams to evaluate configurations of a geothermal-based proton exchange membrane electrolyzer integrated with the organic Rankine cycle [27].

4. Results and Discussion

4.1. Energy Analysis Results

The simulation results are summarized in Table 3. In all three cases, the fuel cells were fed with the same natural gas rate in order to generate 100 kW of electricity; 10 kW was for lighting and control, and 90 kW was for the heat pump loop and EHP. As the rated output power of the adsorption chiller is 72 kW, the power supplied to the heat pump loop was controlled to produce 144 kW of heat. The results show that the power for the heat pump loop was the highest in case A, 39.7 kW, and dramatically decreased to 28.8 and 27.2 kW in cases B and C, respectively. This can be explained by our integrating a cascade loop in case B and an internal heat exchanger in case C. Further explanation can be derived based on the exergy analysis result. The electricity saved in heat pump loops are spent for EHP, leading to more heat and cooling power being produced in cases B and C than in case A. As a result, the PER$_{Cooling}$ decreases from 1.12 in case A to 0.96 in case B and to 0.94 in case C, demonstrating the best performance in case C. The same trend can be seen in terms of heating generation, where PER$_{Heating}$ in case C is 0.78, as opposed to 0.79 in case B and 0.82 in case A.

In addition, the total heating output of case A achieved only 98% of the target power (312 kW), and those of cases B and C both generated output heat higher than the required amount. The values of all streams are listed in Tables A1–A3 in Appendix A.

Primary energy rates of PEMFCs-based tri-generation systems are compared in Table 4. It is shown that the primary energy rates of the proposed systems are significantly lower than those in the studied works. It means that to produce the same amount of the desired energy, the tri-generation systems in this study require less input energy than those in the literature. For instance, in heating mode, the system in case C requires 36.1% less energy than the system developed by Chen et al. [11]. While in cooling mode, the energy saving ratio is 31.4% with the assumption that all the systems are at the same scale. This can be explained by the fact that the proposed systems use a heat pump to

produce high-temperature heat from waste heat. The COP of this single process is 3.63–5.29, calculated from Table 3. In contrast, the other studies in the comparison did not use a heat pump to increase the temperature of the cooling water before storage or use for the adsorption chiller.

Table 3. Energy performance results of the proposed systems.

	Unit	Case A	Case B	Case C
Natural gas input rate	kg/h	19.377	19.377	19.377
PEMFCs output power	kW	100.0	100.0	100.0
Power for lighting and control	kW	10.0	10.0	10.0
Power for heat pump system	kW	39.7	28.8	27.2
Power for EHP	kW	50.3	61.2	62.8
Total cooling power output (Q_C)	kW	241.3	279.6	284.9
Cooling power by EHP (Q_{C1})	kW	132.4	161.1	165.2
Cooling power by adsorption chiller (Q_{C2})	kW	72.0	72.0	72.0
Cooling power by cooling water (Q_{C3})	kW	36.9	46.5	47.7
Total heating power output (Q_H)	kW	305.2	340.3	345.1
Heating power by EHP (Q_{H1})	kW	161.2	196.3	201.1
Heat power by heat pump loop (Q_{H2})	kW	144.0	144.0	144.0
$PER_{Cooling}$	-	1.12	0.96	0.94
$PER_{Heating}$	-	0.82	0.79	0.78

Table 4. Comparison of primary energy rate of tri-generation systems.

Case Study	Primary Energy Rate	Remark
Baniasadi et al. [10]	1.25–1.35	Overall COP 0.74–0.80
Chen et al. [11]	1.22–1.43	Overall COP 0.70–0.82
This study	0.78–0.94	Results of case C

4.2. Exergy Analysis Results

As all three proposed layouts differ only in terms of the heat pump loop design, exergy analysis was only carried out for heat pump loops for their comparison. In addition, exergy destruction was quantified and located for performance improvement. In this study, the exergy of fuel for the total heat pump loop is defined as the sum of exergy input for all pumps and compressors in the loop. In other words, the exergy of fuel is equal to the amount of electricity provided to the heat pump loop. The total destroyed exergy is the sum of the exergy destruction for each component.

The exergy flow diagram within the case A system is shown in Figure 5. At the PEMFCs, 279 kW of exergy is supplied from natural gas for generating 100 kW electricity, and 154.9 kW exergy is destroyed or lost. The cooling water receives 34.3 kW of exergy and brings it to the main evaporator, EV1, where exergy is transferred to the heat pump loop. However, at EV1, more than 80% of the exergy is destroyed because of the large difference in temperature: 55 °C for the water stream on the hot side and 9.4 °C for the refrigerant stream on the cold side. As a result, the exergy of the refrigerant flow through EV1 increases by only 2.1 kW. The exergy flow of 23.1 kW takes place in C1, where 39.5 kW of electricity is supplied to the system through compression work. The hot compressed refrigerant flows to condenser CD1, where its exergy is transferred to 65 °C water from P2. As a result, the refrigerant is condensed while the water experiences an increase in temperature to 70 °C and then enters the adsorption chiller. The exergy flow again decreases in expansion valve V1. As the flow pressure drops from 20 to 3.7 bar, 6.9 kW of exergy is destroyed. The exergy flow is increased by 1.1 kW at EV2 before arriving at EV1 with the completion of a single cycle.
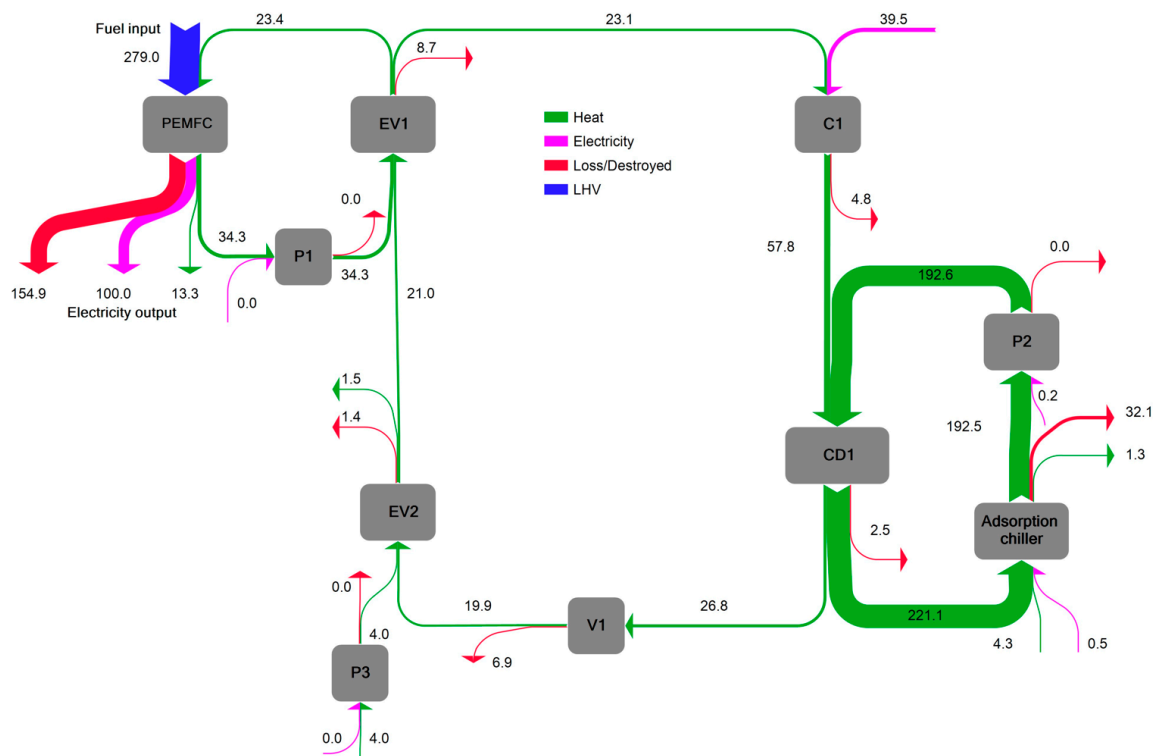
Figure 5. Sankey diagram of exergy flow within the case A system.

Figure 6 presents the exergy flow diagram for the case B system. The hot water that flows from the adsorption chiller absorbs the same amount of exergy as that in case A, increasing from 192.6 to 221 kW. However, thanks to the cascade heat pump loop, the compression ratio of C1 decreases, leading to a reduction in the amount of electricity consumption: 19.2 kW for C1 and 9.2 kW for C2. The power consumption of other compressors and pumps is negligible. Due to the cascade heat pump loop, the difference in pressure at V1 is also reduced, decreasing the amount of destroyed exergy. In addition, a decrease in the destruction exergy ratio in EV1 allows the refrigerant flow to gain more heat through EV1—8.8 kW in case B as opposed to only 2.1 kW in case A.
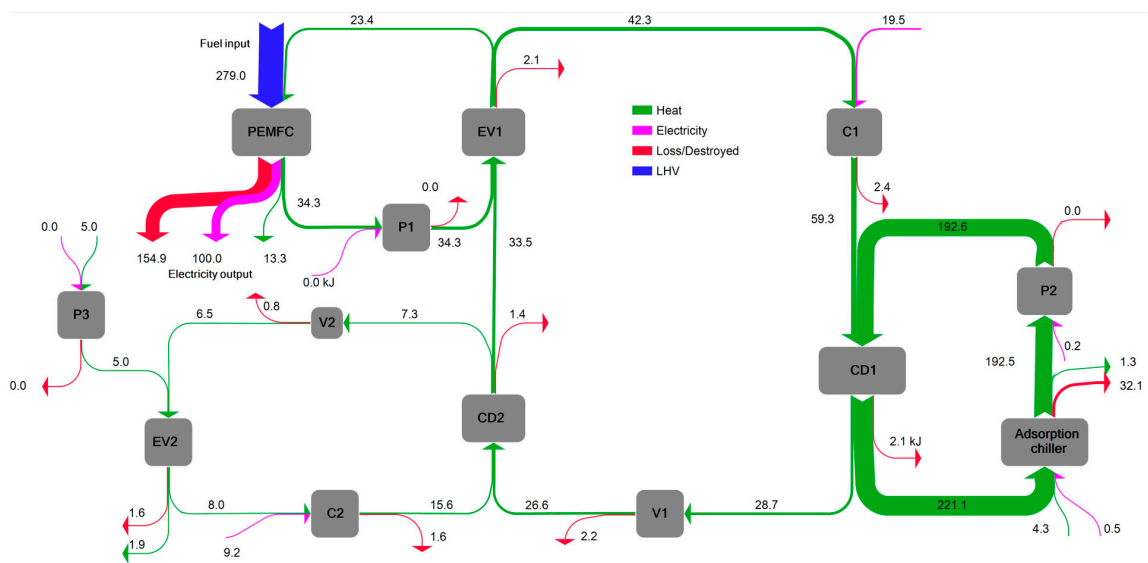
Figure 6. Sankey diagram of exergy flow within the case B system.

Figure 7 shows the exergy flow diagram of case C. Compared with case B, 1.2 kW less electricity is required for C2; the same amounts are supplied for C1 and P2. As a result, the case C system has higher exergy efficiency than the case B system.

Figure 7. Sankey diagram of exergy flow within the case C system.

The total exergy destruction ratios of the three proposed systems are described in Figure 8. The exergy destruction in case A accounts for 61.44% of the fuel exergy, and the proportion of destruction in cases B and C is only 49.18% and 46.60%, respectively. The results clearly reflect the effects of improvements made in cases B and C.

Figure 8. Total exergy destruction of the three proposed systems.

Figure 9 summarizes the exergy destruction ratio, y_k, which is the ratio of the amount of destroyed exergy in each component to the total fuel exergy. Overall, the exergy destruc-

tion in the pumps can be neglected. In case A, most the exergy destruction occurs in EV1, accounting for 22.01% of total fuel exergy due to a large difference in temperature between the hot and cold sides. In case B, the low-temperature refrigerant stream gains much heat from the cascade loop and increases in temperature before entering EV1. Consequently, the exergy destruction ratio here was significantly reduced to 7.16%. Similarly, thanks to an internal heat exchanger in case C, the low-temperature refrigerant stream can recuperate heat from the 70 °C refrigerant flow. As a result, the exergy destruction ratio in EV1 accounts for only 7.47% of the total fuel exergy. The second remarkable portion of exergy destruction occurs at the expansion valves. In case A, 17.34% of the exergy of fuel is destroyed at V1 because the pressure drops from 20 to 3.7 bar. In case B, due to the appearance of a cascade loop, the low side of V1 is set to 9 bar, and at V2 in the cascade loop, the pressure drops from 11 to 3.7 bar. The decrease in pressure ratio at the expansion valves reduces exergy destruction. Subsequently, both valves are responsible for 10.37% of the fuel exergy being destroyed, which is 7% less than that in case A. In case C, two-thirds of the refrigerant drops in pressure from 20 to 9 bar in V1, and the remaining one-third drops to 3.7 bars in V2 in order to mitigate exergy destruction through pressure loss. Consequently, only 8.99% of the fuel exergy is destroyed through expansion valves in case C, the lowest value of the three cases.
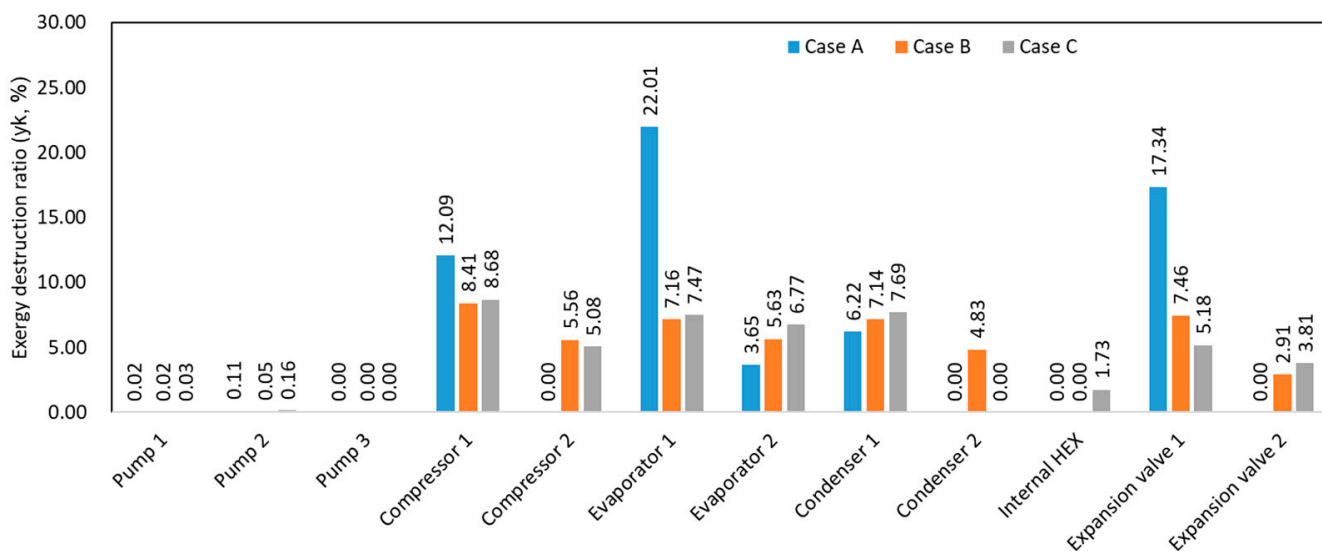

Figure 9. Exergy destruction ratio.

The detailed exergy calculation results for all cases are listed in Appendix A Tables A4–A6.

5. Conclusions

In this study, three different layouts of a heat pump loop integrated into a tri-generation system for a greenhouse were proposed, evaluated, and compared: the first layout uses a simple heat pump loop (case A), the second layout includes a cascade heat pump loop (case B), and the third layout has an internal heat exchanger (case C). System simulation was performed using appropriate assumptions and parameter settings. To facilitate understanding, the quantification and allocation of thermodynamic inefficiency and exergy destruction were determined using an exergy-based analysis method.

The main results can be summarized as follows:

1. The proposed systems show the superiority of energy efficiency over those in other relevant works because of the use of a heat pump to utilize the waste heat from PEMFCs. In detail, it can reduce energy consumption by 36.1% and 31.4% in heating and cooling modes, respectively, compared with relevant studies.

2. All proposed systems essentially matched the demands for power and heat of the 4800 m^2 greenhouse except the heating mode in case A, using a simple heat pump. In this case, the generated heat was approximately 98% of the required heat.
3. Case C, with an internal heat exchanger, has the best performance with a PERs of 0.94 and 0.79 in cooling and heating modes, respectively. However, there is little difference in energy performance between cases B and C. Economic and environmental analyses should be conducted in ongoing studies for more comprehensive comparison of configurations.
4. The exergy-based analysis clearly showed that exergy is mostly destroyed at evaporators and expansion valves. In cases B and C, the difference in pressure at the expansion valve is reduced by the cascade loop and the internal heat exchanger, respectively. In addition, a higher pressure in the evaporator allows for a warmer refrigerant stream, leading to a lower difference in temperature between the cold refrigerant and hot water streams. Decreases in both the pressure difference at the expansion valves and the temperature difference in the evaporator significantly reduced exergy destruction in the systems of cases B and C compared with that of case A.

Author Contributions: Conceptualization, T.B, Y.-S.K. and D.-K.L.; methodology, T.B., Y.-S.K. and D.-K.L.; software, T.B.; validation, T.B. and D.-K.L.; formal analysis, T.B. and Y.-S.K.; investigation, T.B. and Y.-S.K.; resources, Y.-S.K., K.-Y.A. and S.-M.L.; data curation, T.B., K.-Y.A. and S.-M.L.; writing—original draft preparation, T.B.; writing—review and editing, Y.-S.K., K.-Y.A. and S.-M.L.; supervision, Y.-S.K.; project administration, Y.-S.K. and S.-M.L.; funding acquisition, Y.-S.K., K.-Y.A. and S.-M.L. All authors have read and agreed to the published version of the manuscript.

Institutional Review Board Statement: Not applicable.

Informed Consent Statement: Not applicable.

Data Availability Statement: Not applicable.

Conflicts of Interest: The authors declare no conflict of interest.

Appendix A

Table A1. Stream data of case A.

Stream	P	T	M	Q
	bar	°C	kg/s	kW
01	1.00	25.00	0.01	0.29
02	1.00	25.00	0.26	6.50
03	0.97	82.05	0.32	28.23
04	1.00	45.00	1.68	315.77
05	1.05	55.00	1.68	385.78
06	1.00	55.00	1.68	385.77
07	1.10	55.00	1.68	385.80
08	1.07	45.00	1.68	315.77
09	1.00	25.00	0.88	92.34
10	1.05	25.00	0.88	92.34
11	1.00	15.00	0.88	55.51

Table A1. *Cont.*

Stream	P	T	M	Q
12	1.00	65.00	6.88	1872.33
13	1.00	65.00	6.88	1872.33
14	1.15	65.00	6.88	1872.48
15	1.10	70.00	6.88	2016.50
16	3.60	13.73	0.56	290.40
17	20.00	99.78	0.56	329.40
18	20.00	70.00	0.56	185.38
19	20.00	70.00	0.56	185.38
20	3.70	9.78	0.56	185.38
21	3.65	9.37	0.56	220.37
30				100.00
31				50.33
32				49.67
33				39.67
34				10.00

Table A2. Stream data of case B.

Stream	P	T	M	Q
	bar	°C	kg/s	kW
01	1.00	25.00	0.01	0.29
02	1.00	25.00	0.26	6.50
03	0.97	82.05	0.32	28.23
04	1.00	45.00	1.68	315.77
05	1.05	55.00	1.68	385.78
06	1.00	55.00	1.68	385.77
07	1.08	55.00	1.68	385.79
08	1.05	45.00	1.68	315.77
09	1.00	25.00	1.11	116.26
10	1.03	25.00	1.11	116.27
11	1.00	15.00	1.11	69.89
12	1.00	65.00	6.90	1876.42
13	1.00	65.00	6.90	1876.42
14	1.05	65.00	6.90	1876.47
15	1.00	70.00	6.90	2020.76
16	8.90	45.48	0.60	323.65
17	20.00	89.26	0.60	342.91
18	19.97	70.00	0.60	198.62
19	19.97	70.00	0.60	198.62
20	9.00	39.62	0.60	198.62
21	8.95	39.41	0.60	253.63
22	3.65	17.22	0.19	100.29
23	11.00	70.55	0.19	108.92
24	11.00	45.00	0.19	53.92
25	11.00	45.00	0.19	53.92
26	3.70	9.78	0.19	53.92
30				100.00
31				61.23
32				38.77
33				28.77
34				10.00

Table A3. Stream data of case C.

Stream	P	T	M	Q
	bar	°C	kg/s	kW
01	1.00	25.00	0.01	0.29
02	1.00	25.00	0.26	6.50
03	0.97	82.05	0.32	28.23
04	1.00	45.00	1.68	315.77
05	1.05	55.00	1.68	385.78
06	1.00	55.00	1.68	385.77
07	1.10	55.00	1.68	385.80
08	1.07	45.00	1.68	315.77
09	1.00	25.00	1.14	119.62
10	1.03	25.00	1.14	119.62
11	1.00	15.00	1.14	71.91
12	1.00	65.00	6.88	1872.33
13	1.00	65.00	6.88	1872.33
14	1.15	65.00	6.88	1872.48
15	1.10	70.00	6.88	2016.55
16	8.90	39.20	0.40	212.17
17	8.90	47.88	0.59	320.16
18	20.00	91.55	0.59	339.38
19	20.00	70.00	0.59	195.31
20	20.00	70.00	0.40	132.42
21	20.00	70.00	0.40	132.42
22	9.00	39.62	0.40	132.42
23	8.95	39.41	0.40	142.15
24	20.00	70.00	0.19	62.90
25	19.97	44.53	0.19	53.17
26	3.70	9.78	0.19	53.17
27	3.65	24.73	0.19	100.88
28	8.90	67.39	0.19	107.99
30				100.00
31				62.78
32				37.22
33				27.22
34				10.00

Table A4. Exergy calculation results of case A.

	$E_{P,k}$ kW	$E_{P,k}$ kW	$E_{D,k}$ kW	ε_k %	y_k %
Pump 1	0.03	0.02	0.01	70.99	0.02
Pump 2	0.16	0.11	0.05	71.49	0.11
Pump 3	0.01	0.00	0.00	72.37	0.00
Compressor 1	39.48	34.68	4.80	87.85	12.09
Evaporator 1	10.83	2.10	8.73	19.41	22.01
Evaporator 2	2.51	1.07	1.45	42.47	3.65
Condenser 1	30.97	28.51	2.47	92.04	6.22
Expansion valve 1	-		6.88	-	17.34
Total system	39.67	-	24.37	-	61.44

Table A5. Exergy calculation results of case B.

	$E_{P,k}$ kW	$E_{P,k}$ kW	$E_{D,k}$ kW	ε_k %	y_k %
Pump 1	0.02	0.01	0.01	70.99	0.02
Pump 2	0.05	0.04	0.02	71.69	0.05
Pump 3	0.00	0.00	0.00	72.23	0.00
Compressor 1	19.49	17.07	2.42	87.59	8.41
Compressor 2	9.19	7.6	1.60	82.59	5.56
Evaporator 1	10.83	8.78	2.06	81.00	7.16
Evaporator 2	3.16	1.54	1.62	48.76	5.63
Condenser 1	30.61	28.56	2.05	93.29	7.14
Condenser 2	8.30	6.91	1.39	83.27	4.83
Expansion valve 1	-	-	2.15	-	7.46
Expansion valve 2	-	-	0.84	-	2.91
Total system	28.77	-	14.15	-	49.18

Table A6. Exergy calculation results of case C.

	$E_{P,k}$ kW	$E_{P,k}$ kW	$E_{D,k}$ kW	ε_k %	y_k %
Pump 1	0.03	0.02	0.01	70.99	0.03
Pump 2	0.16	0.11	0.04	71.69	0.16
Pump 3	0.00	0.00	0.00	72.23	0.00
Compressor 1	19.46	17.06	2.40	87.66	8.68
Compressor 2	8.02	6.6	1.40	82.49	5.08
Evaporator 1	10.83	8.77	2.07	80.91	7.47
Evaporator 2	3.23	1.35	1.87	41.88	6.77
Condenser 1	30.65	28.52	2.13	93.06	7.69
Internal HEX	1.69	1.21	0.48	71.65	1.73
Expansion valve 1	-	-	1.43	-	5.18
Expansion valve 2	-	-	1.05	-	3.81
Total system	27.67	-	12.89	-	46.60

References

1. Ghazanfari Holagh, S.; Abdollahi Haghghi, M.; Chitsaz, A. Which methane-fueled fuel cell is of superior performance in CCHP applications; solid oxide or molten carbonate? *Fuel* **2022**, *312*, 122936. [CrossRef]
2. Milewski, J.; Badyda, K. Tri-generation systems based on hightemperature fuel cells. In Proceedings of the International Conference on Power Engineering (ICOPE), Kobe, Japan, 16 November 2009.
3. Raj Singh, U.; Sai Kaushik, A.; Sekhar Bhogilla, S. A novel renewable energy storage system based on reversible SOFC, hydrogen storage, Rankine cycle and absorption refrigeration system. *Sustain. Energy Technol. Assess.* **2022**, *51*, 101978. [CrossRef]
4. Rinaldi, G.; McLarty, D.; Brouwer, J.; Lanzini, A.; Santarelli, M. Study of CO_2 recovery in a carbonate fuel cell tri-generation plant. *J. Power Sources* **2015**, *284*, 16–26. [CrossRef]
5. Roushenas, R.; Zarei, E.; Torabi, M. A novel trigeneration system based on solid oxide fuel cell-gas turbine integrated with compressed air and thermal energy storage concepts: Energy, exergy, and life cycle approaches. *Sustain. Cities Soc.* **2021**, *66*, 102667. [CrossRef]
6. Tse, L.K.C.; Wilkins, S.; McGlashan, N.; Urban, B.; Martinez-Botas, R. Solid oxide fuel cell/gas turbine trigeneration system for marine applications. *J. Power Sources* **2011**, *196*, 3149–3162. [CrossRef]
7. Wang, S.; Lu, X.; Mei, S.; Zhu, Y. Solid Oxide Fuel Cell Trigeneration System and Performance Analysis. *Tianjin Daxue Xuebao (Ziran Kexue Yu Gongcheng Jishu Ban)/J. Tianjin Univ. Sci. Technol.* **2021**, *54*, 1061–1069. [CrossRef]

8. Loreti, G.; Facci, A.L.; Baffo, I.; Ubertini, S. Combined heat, cooling, and power systems based on half effect absorption chillers and polymer electrolyte membrane fuel cells. *Appl. Energy* **2019**, *235*, 747–760. [CrossRef]
9. DOE. *Quadrennial Technology Review 2015*; DOE: Washington, DC, USA, 2015.
10. Baniasadi, E.; Toghyani, S.; Afshari, E. Exergetic and exergoeconomic evaluation of a trigeneration system based on natural gas-PEM fuel cell. *Int. J. Hydrogen Energy* **2017**, *42*, 5327–5339. [CrossRef]
11. Chen, X.; Gong, G.; Wan, Z.; Luo, L.; Wan, J. Performance analysis of 5 kW PEMFC-based residential micro-CCHP with absorption chiller. *Int. J. Hydrogen Energy* **2015**, *40*, 10647–10657. [CrossRef]
12. Khan, M.S.; Mubeen, I.; Jingyi, W.; Zhang, Y.; Zhu, G.; Yan, M. Development and performance assessment of a novel solar-assisted multigenerational system using high temperature phase change material. *Int. J. Hydrogen Energy* **2022**, *47*, 26178–26197. [CrossRef]
13. Bellos, E.; Lykas, P.; Tzivanidis, C. Pumped Thermal Energy Storage System for Trigeneration: The Concept of Power to XYZ. *Appl. Sci.* **2022**, *12*, 970. [CrossRef]
14. Kim, Y.J.; Yang, L.; Entchev, E.; Cho, S.; Kang, E.C.; Lee, E.J. Hybrid Solar Geothermal Heat Pump System Model Demonstration Study. *Front. Energy Res.* **2021**, *9*, 778501. [CrossRef]
15. Najafi, B.; Casalegno, A.; Intini, M.; De Antonellis, S.; Rinaldi, F. A trigeneration system based on polymer electrolyte fuel cell and desiccant wheel—Part A: Fuel cell system modelling and partial load analysis. *Energy Convers. Manag.* **2015**, *106*, 1450–1459. [CrossRef]
16. Samjungtech. Absorption Chiller & Fan Coil Unit. Available online: http://www.samjungtech.com/renew_2016/eng/data/busi02_catalog.pdf (accessed on 6 October 2022).
17. Javadi, M.A.; Khodabakhshi, S.; Ghasemiasl, R.; Jabery, R. Sensivity analysis of a multi-generation system based on a gas/hydrogen-fueled gas turbine for producing hydrogen, electricity and freshwater. *Energy Convers. Manag.* **2022**, *252*, 115085. [CrossRef]
18. Mitchell, J.; Braun, J.E. *Principles of Heating, Ventilation, and Air Conditioning in Buildings*; John Wiley & Sons: Hoboken, NJ, USA, 2012.
19. Bellos, E.; Tzivanidis, C. Investigation of the Environmentally-Friendly Refrigerant R152a for Air Conditioning Purposes. *Appl. Sci.* **2019**, *9*, 119. [CrossRef]
20. LG. Inverter scroll chiller. Available online: https://www.lg.com/gr/leaflets/170502_ISChiller_Catalog_EU.PDF (accessed on 6 October 2022).
21. Ge, Y.; Tassou, S.; Chaer, I.; Sugiartha, N. Performance evaluation of a tri-generation system with simulation and experiment. *Appl. Energy* **2009**, *86*, 2317–2326. [CrossRef]
22. Havelský, V. Energetic efficiency of cogeneration systems for combined heat, cold and power production. *Int. J. Refrig.* **1999**, *22*, 479–485. [CrossRef]
23. Kong, X.-Q.; Wang, R.-Z.; Li, Y.; Wu, J.-Y. Performance research of a micro-CCHP system with adsorption chiller. *J. Shanghai Jiaotong Univ. (Science)* **2010**, *15*, 671–675. [CrossRef]
24. Murugan, S.; Horák, B. Tri and polygeneration systems—A review. *Renew. Sustain. Energy Rev.* **2016**, *60*, 1032–1051. [CrossRef]
25. Ziegler, F.; Riesch, P. Absorption cycles. A review with regard to energetic efficiency. *Heat Recovery Syst. CHP* **1993**, *13*, 147–159. [CrossRef]
26. Javadi, M.; Jafari Najafi, N.; Khalili Abhari, M.; Jabery, R.; Pourtaba, H. 4E analysis of three different configurations of a combined cycle power plant integrated with a solar power tower system. *Sustain. Energy Technol. Assess.* **2021**, *48*, 101599. [CrossRef]
27. Ranjbar Hasani, M.; Nedaei, N.; Assareh, E.; Alirahmi, S.M. Thermo-economic appraisal and operating fluid selection of geothermal-driven ORC configurations integrated with PEM electrolyzer. *Energy* **2023**, *262*, 125550. [CrossRef]